ELSEVIER

Journal of Alloys and Compounds 230 (1995) 1–12

Journal of ALLOYS AND COMPOUNDS

Synthesis, structures and properties of cubic R_3In and R_3InZ phases (R = Y, La; Z = B, C, N, O)

The effect of interstitial Z on the superconductivity of La_3In

Jing-Tai Zhao, Zhen-Chao Dong, J.T. Vaughey, Jerome E. Ostenson, John D. Corbett*

Ames Laboratory-DOE, and Department of Chemistry, Iowa State University, Ames, IA 50011, USA

Received 15 July 1994; in final form 24 May 1995

Abstract

Samples of La_3In, Y_3InC_x and La_3InZ_x for $0.3 \leq x \leq 1.5$, Z = C and O, La_3InB_x for $0.7 \leq x \leq 1.5$, and La_3InN were synthesized in welded Ta containers by powder sintering, fusion and annealing techniques. Y_3In and La_3Ga could not be obtained. All of the R_3InZ_x examples were single phase between $x \approx 0.3$–0.5 and $x \approx 1.0$ and had the inverse perovskite structure (stuffed Cu_3Au). Single crystal refinements for Y_3InC and La_3InN confirmed the type and stoichiometry ($Pm\bar{3}m$, $a = 4.9023(7)$ Å, 5.102(1) Å, and $R(F)/R_w = 1.1/1.3\%$, 2.2/2.4% respectively). Magnetic susceptibilities measured for both normal and superconducting states showed $T_c \approx 10$ K and $10^4\chi_{RT} \approx 4$ emu mol^{-1} were retained through the B and O series, with some enhancement of density and supercurrent shielding for B and a reduction of both for O. The absence of superconductivity (greater than 2 K) for Y_3InC, La_3InC and La_3InN parallels their $10^4\chi_{RT}$ values of less than or equal to 2 emu mol^{-1}; the temperature dependencies of χ for these were also notably less than for the superconductors. These last phases are also more brittle. Extended Hückel band calculations indicated appreciable In and B (La–In and La–B) contributions at E_F for La_3InB. Thereafter, the La–Z bonding states rapidly fall in energy as does the amount of La–In bonding at E_F, the last returning somewhat with the electron-richest oxygen interstitial. The decrease in T_c with increasing x in La_3InC_x parallels a decrease in densities-of-states at E_F.

Keywords: R_3InZ compounds; Interstitials; Synthesis; Structure; Superconductivity

1. Introduction

It has been well established that compounds with the Cu_3Au type of structure have significant versatility in accepting second-period interstitial atoms [1]. Compounds between the rare-earth metals (R) and the Al family (or triel Tr) elements Ga and In also continue to attract us as means to define and to understand structures, valence and bonding characteristics, and physical properties. These characteristics led us to investigate two families of R_3In and R_3InZ compounds in which the centered interstitial Z produces an inverse perovskite structure from the Cu_3Au-type host. The empty R_3In phases are known for R = La–Sm but not for Y, Gd and beyond [2], while a variety of R_3TrC phases have been produced for Tr = Al–Tℓ (and others) [1,3,4] as well as few Nd_3TrN examples [5]. All of these assignments have been based only on powder pattern evidence, and some of these R–Tr combinations occur only as ternary compounds. Single phase products were not always achieved, so some uncertainties remained about the limiting compositions, although many of the carbides were considered to be deficient in carbon. However, these studies included little information about properties other than the unit cell types and dimensions. The chemistry and physics of such products must be very rich owing to their potential of accommodating different interstitial atoms.

The compound La_3In has been reported to be a strongly-coupled superconductor with transition temperature $T_c = 9.5$ K [6,7]. Although the magnitude of the superconducting transition temperature itself is not very promising, the interstitial chemistry of a phase with such special properties provides some very interesting prospects that have apparently not been investi-

* Corresponding author.

SSDI 0925-8388(95)01909-X

gated before. Here we report our syntheses, structure determinations (or confirmations), some property measurements and band calculations for Y_3InC and for La_3InZ with Z = B, C, N, O or nothing.

2. Experimental

2.1. Materials

The La rod used was an Ames Laboratory product (99.999%) with principal impurities (in atom ppm) of O, 190; N, 128; C, 34; F, 80 and Fe, 7.6. The Y metal used was also a comparable Ames Lab product. The metals were scraped free of any colored surfaces in a He-filled glovebox before pieces were cut and weighed. The other reactants used were as follows: B (99.5%), Aesar; In (99.9999%), Johnson Matthey; C (spectroscopic grade), Union Carbide; La_2O_3 (99.999%), Ames Laboratory.

2.2. Syntheses

The powder sintering method, and either direct reactions in tube furnaces to 1100°C in a high temperature vacuum furnace [8], or induction heating were generally used in the syntheses of the ternary compounds. Sealed Ta containers were used throughout, and these were either jacketed in silica in tube furnace reactions or utilized directly in the high vacuum systems within the other furnaces. Quantification of products for reactions of known composition by sensitive Guinier powder pattern methods is an important means of establishing product compositions.

The binary La_3In (melting point about 816°C, liquidus about 860°C [9]) was prepared by arc-melting and then annealed under conditions described in Table 1. Guinier powder patterns of such products showed them to be single phase Cu_3Au type. Since the compound is not brittle, only small pieces could be used to obtain 'powder' patterns. For the ternary phases, direct fusion of either the elements or the appropriate compounds followed by annealing did not always produce high quality, single phase products, in some cases because of apparent loss or dispersion of the interstitial source during the process. Therefore, La_3In or an appropriate neighboring composition prepared by direct reaction in welded Ta tubes was subsequently hydrogenated in order to gain a finely powdered reactant. Such a process gave mixtures of LaH_{2+x} and In according to powder patterns taken after annealing at 140°C for 24 h. These powdered

Table 1
Composition of and conditions for R_3InZ reactions and the yields and unit cell parameters of the cubic products

Nominal composition	Reaction conditions[a]	Yield of cubic $La_3In(Z)$ (%)	$a(\sigma)$[b] (Å)	$V(\sigma)$ Å^3
La_3In	(a)	~100	5.089 (7)	131.8 (5)
$La_3InB_{0.7}$	(b)[c]	~100	5.084 (2)	131.4 (1)
La_3InB	(b)[c]	~100	5.095 (1)	132.26 (9)
La_3InB	(c)	>90	5.071 (2)	130.4 (2)
$La_3InB_{1.5}$	(b)[c]	>80	5.084 (2)	131.4 (2)
$La_3InC_{0.3}$	(b)[c]	~100	5.157 (1)	137.18 (9)
$La_3InC_{0.7}$	(b)[c]	~100	5.1728 (7)	138.41 (5)
La_3InC	(b)[c]	>90	5.1971 (8)	140.37 (7)
La_3InC	(c)	>90	5.193 (2)	140.0 (2)
$La_3InC_{1.5}$	(b)[c]	>90	5.194 (1)	140.16 (8)
La_3InN	(d)[c]	>90	5.102 (1)	132.8 (1)
La_3InN	(e)[c]	~100	5.1095 (9)	133.39 (7)
$La_3InO_{0.3}$	(f)	~100	5.2087 (5)	141.32 (4)
$La_3InO_{0.7}$	(f)	~100	5.209 (2)	141.3 (1)
La_3InO	(f)	>90	5.187 (3)	139.5 (3)
La_3InO	(c)	>80	5.196 (2)	140.3 (2)
$La_3InO_{1.5}$	(f)	>70	5.2053 (9)	141.04 (7)
$Y_3InC_{0.3}$	(f)[c]	~70[e]	4.879 (1)	116.14 (7)
$Y_3InC_{0.7}$	(f)[c]	>90	4.8901 (6)	116.94 (4)
Y_3InC	(f)[c]	>95	4.9001 (5)	117.66 (4)
Y_3InC[d]	(c)	>70	4.9023 (7)	117.81 (5)
$Y_3InC_{1.5}$	(f)[c]	>70	4.8998 (7)	117.63 (5)

[a] Reaction conditions (all in °C). (a) Arc-melting; tube furnace: 700, 0.1 h; 30/h → 790, 50 h; −10/h → 560 → RT. (b) HT furnace: 1 h → 800, 2 h; 0.5 h → 1300, 2 h; 0.5 h → 800, 0.5 h; 2 h → 650; 5 h → RT. (c) Induction furnace: →1350, 2 h → RT. Tube furnace: →400, 18 h → 650, 500 h → RT. (d) Tube furnace: →350, 24 h → 550, 72 h → 900, 0.5 h; 20/h → 1100, 72 h; −2/h → 760 → RT. (e) Tube furnace: 5 h → 1080, 300 h; −5/h → 700, 24 h; −20/h → 600 → RT. (f) HT furnace: 1 hr → 800, 0.5 h; 0.5 h → 1350, 6 h; 0.5 h → 920, 12 h; 8 h → RT.

[b] Guinier data with Si as internal standad, $\lambda = 1.540\,562$ Å.

[c] Sintering of pelletized powders.

[d] Source of single crystal for diffraction.

[e] Plus approximately 30% La_2In.

mixtures were subsequently mixed with the appropriate elemental B, C, LaN or La_2O_3, pressed into pellets, sealed within Ta containers, and heated slowly over some hours under dynamic vacuum (10^{-5} Torr) up to the neighborhood of 1300°C where a liquid product is present. Hydrogen pumps out of the container during this step since Ta is transparent to hydrogen at elevated temperatures. The product was then annealed at lower temperatures, as specified.

The binary compounds Y_2In and La_2In employed for powder sintering with RN to gain Y_3InN and La_3InN were prepared by arc-melting and then ground into powders. The R_2In products were not annealed so that defects and stress in the samples would increase their reactivity. Powdered YH_x was also used with Y_2In in pellet reactions in attempts to achieve Y_3In as well as when C was added to gain Y_3InC. The YH_x and RN phases were prepared in-house from the elements.

Table 1 lists the reaction conditions and yields for different syntheses of diverse R_3InZ phases, R = La, Y, Z = B, C, N, O, as well as the lattice dimensions and cell volumes of the cubic products. Some routes were clearly more successful than others, powder sintering for the borides and carbides especially. Yields were estimated on the basis of line intensities in observed powder patterns relative to those calculated for known structures. Extra diffraction lines in the patterns of products from some reactions that gave appreciably less than 100% yields of the cubic R_3InZ could not be assigned to the simple binary phases. However, La_2In was evident in products with overall compositions $La_3InZ_{1.5}$, Z = B, C, O. This is consistent with the loss of La (as LaZ_x) that usually occurs either with excess nonmetal Z or when the interstitial product does not form, as established in many La_5Ge_3Z and La_5Pb_3Z studies [10,11]. Mixtures of cubic R_3In and R_3InZ were never seen, indicating that samples of La_3InZ_x for Z = B, C, O and of Y_3InC_x were single phase for at least approximately $0.3 \leq x \leq 1$ ($0.7 \leq x \leq 1$ for B) and therefore nonstoichiometric (solid solutions) up to $x \approx 1.0$. The $0 < x < 0.3$ regions were not investigated, however. The series with Z = B, C, O are also each internally consistent. Note that the quantitative yields, or nearly so, of known phases from these sealed tube reactions afford strong evidence regarding the stoichiometry of the products. The Y_3InC, La_3InC and La_3InN products are brittle; La_3InB and La_3InO tend to be more ductile, shiny and metal-like and therefore more difficult to powder.

2.3. Characterization

The products were characterized by powder and, for some, single crystal X-ray diffraction methods at room temperature, as well as by magnetic susceptibility and a few conductivity measurements as a function of temperature. The procedures are the same as those used for studies of the binary rare-earth-metal gallides that have been described in detail elsewhere [12]. X-ray powder films obtained with the aid of an Enraf–Nonius Guinier camera and Cu $K\alpha_1$ radiation were used for phase identification. (The detection limit is about 2–4%.) Comparison of the films with powder patterns calculated for phases with known structures were used for indexing and for estimations of yields; unit cell parameters were refined by least squares means from the 2θ values measured with the aid of NIST silicon as an internal standard. Some unusual, apparently composition-invariant characteristics of the boron products (below) also led us to examine the composition and phase distributions in La_3InB_x samples with the aid of a vacuum transfer device from Oxford Instruments and a JEOL JSM-840 SEM equipped with a KEVEX EDX system.

Single crystals of La_3InN and Y_3InC picked from crushed bulk samples were mounted in glass X-ray capillaries inside a N_2-filled glovebox. The crystals were checked by Laue or oscillation photographs prior to data collections. The latter were made with the aid of an Enraf–Nonius CAD-4 diffractometer and monochromated Mo $K\alpha$ radiation. The routine indexing and cell reduction procedures gave primitive cubic cells. The structure refinements were carried out with an assumed Cu_3Au type structure as the model, and the centered location of the interstitials was confirmed by difference Fourier maps. The structure refinements were carried out with program package TEXSAN [13]. The absorption corrections were made empirically according to ψ-scan curves of three strong reflections with different θ values and, later, through empirical calculations by DIFABS [14]. Anomalous dispersion of the elements was taken into account during the refinements. Some experimental details of the structure refinements are listed in Table 2, the atomic positional and displacement parameters are in Table 3, and interatomic distances are summarized in Table 4. The F_o/F_c data are available from J.D.C.

Samples for magnetic susceptibility and superconductivity measurements were held between two fused silica rods that were in turn fixed inside a silica tube filled with He and sealed at both ends. The magnetic susceptibility measurements were carried out at 3 T between 6 and 300 K for the normal state with the aid of a Quantum Design SQUID magnetometer and were corrected for standard diamagnetic core contributions. The superconducting state data were measured at 50 Oe, usually after cooling to 2 K in zero field. The electrical resistivity of La_3InC was measured between 100 and 290 K on an improved apparatus for the Q-method [15].

Table 5 lists T_c, supercurrent shielding, and χ_{293} data for many of the samples described in Table 1. In addition, μ_{eff} values based on Curie–Weiss fits be-

Table 2
Experimental detail of refinements of Y_3InC and La_3InN compounds in the antiperovskite-type structure

Compound	Y_3InC	La_3InN
Unit cell: a (Å)	4.9023 (7)	5.102 (1)
V (Å^3)	117.81 (5)	132.8 (1)
Space group, Z	$Pm\bar{3}m$ (no. 221), 1	$Pm\bar{3}m$ (no. 221), 1
Formula weight	393.55	545.54
d_{calc} (g cm^{-3})	5.558	6.821
$F(000)$	172	227
μ(Mo K$_\alpha$) (cm^{-1})	414.81	278.17
Transmission range	0.61–1.14	0.56–1.21
No. observed reflections ($I > 3\sigma_I$)	60	61
No. parameters	6	6
Residuals: R_w/R	1.3/1.1	2.4/2.2
Residual peak (+/−, e Å^{-3})	0.7/0.7	1.5/0.8
Sec. extinct coeff. (10^{-5})	2.09 (7)	11.6 (5)

Table 3
Atomic positional and displacement parameters[a] for Y_3InC and La_3InN

Atom	x	y	z	B_{eq}	U_{11}	U_{22}
Y	0	1/2	1/2	0.54 (2)	0.51 (4)	0.78 (2)
In	0	0	0	0.3748 (3)	0.4747 (4)	U_{11}
C	1/2	1/2	1/2	3.033 (5)	3.84 (1)	U_{11}
La	0	1/2	1/2	1.02 (3)	0.93 (5)	1.48 (6)
In	0	0	0	1.0379 (6)	1.3145 (7)	U_{11}
N	1/2	1/2	1/2	1.795 (7)	2.27 (1)	U_{11}

[a] $U_{ii} \times 10^2$. $T = \exp[-2\pi^2(U_{11}h^2a^{*2} + U_{22}k^2b^{*2})]$.

Table 4
Nearest neighbor distances (Å) in Y_3InC and La_3InN

	Y_3InC	La_3InN
R–8R R–4In In–12R	3.4640 (3)	3.6077 (7)
R–2C C–6R	2.4495 (2)	2.5510 (5)

tween 50–100 K and 300 K are given as a means of quantifying the temperature dependencies of χ_M.

2.4 Band calculations

Extended Hückel band calculations were carried out as before [8,10] on La_3In and the four La_3InZ examples using the experimental values of lattice constants and thence the interatomic distances in each. Calculations were made at 220 or more k-points for the ternary phases and 120 for La_3In. The atomic parameters employed were the default values in the program. Crystal orbital overlap population (COOP) analyses [16], that is, overlap-weighted orbital populations for specified atom pairs, were also computed as a function of energy to aid the description of their interactions. Projected atomic contributions in the total DOS will be overestimated for La and understated for In and Z because of the equal partitioning of bonding electrons applied in the Mulliken approximation.

3. Results and Discussion

3.1. Y_3InC

No Y_3In phase has been found previously [2], and we were not able to produce the compound either. Comparison of the yields and unit cell parameters for Y_3InC_x samples, Table 1, leads to the conclusion that the single phase region must be significantly broad, perhaps $0.4–0.5 < x < 1.0$, since the composition $Y_3InC_{0.3}$ contained about 30% Y_2In. The phase is thus an interstitially-stabilized Cu_3Au structure, one that corresponds to an ideal inverse perovskite at the $x = 1$ limit. The structural study of Y_3InC confirmed that the interstitial is present in stoichiometric amounts and is bound in the only reasonable place, the body center within the yttrium octahedron. The Y–C distance, 2.450 Å, compares with 2.50 Å from Slater (atomic) radii [17]. The average Y–C distances in $Y_{10}I_{13}C_2$ [18], Y_4I_5C and $Y_6I_7C_2$ [19], where carbon is also octahedrally bound by yttrium, range between 2.46 and 2.55 Å, but cluster condensation and, particularly, a matrix effect from the large iodine are apt to cause somewhat greater Y–C separations within this group. Nonetheless, the stabilization of the two very different

Table 5
Magnetic properties of R_3InZ phases, R = La, Y

Nominal composition[a]	T_c (K)[b]	Supercurrent shielding (%)[c]	χ_{293} $(10^{-4}$ emu mol$)^{-1}$	μ_{eff} (BM)
La_3In	10	180	3.5	1.86 (3)
$La_3InB_{0.7}$[d]	10	220	4.0	2.05 (2)
La_3InB[d]	10	300	4.6	1.8 (2)
La_3InB	9.5	114	2.2	1.4 (3)
$La_3InC_{0.3}$[d]	9	130	3.5	2.03 (3)
$La_3InC_{0.7}$[d]	3.5	20	2.1	1.72 (5)
La_3InC[d]	—	—	2.0	1.18 (4)
La_3InC	2.6	8[e]	1.7	1.01 (2)
La_3InN[d]	—	—	1.5	—
$La_3InO_{0.3}$	10	200	3.9	2.31 (7)
$La_3InO_{0.7}$	10	130	4.3	3.5 (2)
La_3InO	10	80	4.3	2.76 (7)
La_3InO	9.5	160	3.2	2.6 (2)
$Y_3InC_{0.7}$[d]	—	—	0.9	—
Y_3InC[d]	—	—	1.0	1.10 (2)
Y_3InC	—	—	1.2	—

[a] See Table 1. The order is the same.
[b] For $T_c > 2$ K.
[c] Measured at 50 Oe.
[d] Powder sintering product.
[e] At 1.8 K.

classes of yttrium compounds by carbon and the Y–C bonding within both presumably are closely related. The brittleness of the present carbide samples indicates that polar covalent Y–C bonding probably dominates in the compound, in contrast to the lanthanum boride. Ternary reactions targeted on Y_3InLi, Y_3InN, Y_3InP and Y_3InF did not yield perovskite-type phases.

None of the carbide samples showed bulk superconductivity above 2 K, while the magnetic susceptibilities of $Y_3InC_{0.7}$ and Y_3InC samples, Fig. 1, appear to be Pauli paramagnetic in character and relatively small at room temperature. One might argue that one should classify the stoichiometric Y_3InC as another metallic Zintl (valence) phase [20] since oxidation states in the compound give a zero sum when these are assigned at the closed-shell limits, $(Y^{+3})_3In^{-5}C^{-4}$. This of course is an unrealistic charge disposition. In fact, band calculations described later for the lanthanum analogue do not support such an extreme electron association with indium.

3.2. La_3InZ

La_3In: The lattice constant found is in good agreement with that given by McMasters and Gschneidner, 5.0854(2) Å [9]. Magnetic susceptibilities as a function of T for La_3In, along with those of all La_3InZ, are shown in Fig. 2. The La_3In results are Pauli-like in magnitude but only roughly temperature-independent; the appreciable rise in χ with decreasing temperature

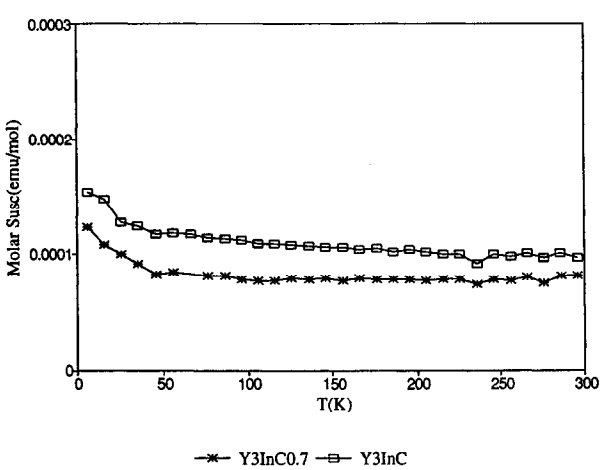

Fig. 1. Molar magnetic susceptibilities of $Y_3InC_{0.7}$ and Y_3InC as a function of temperature.

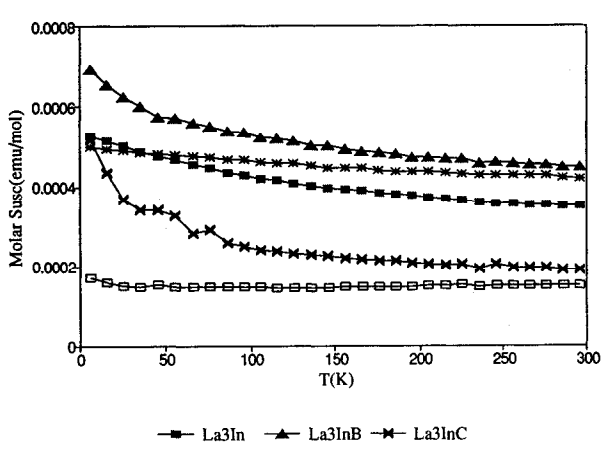

Fig. 2. Magnetic susceptibilities as a function of temperature for, from top to bottom, La_3InB, La_3InO, La_3In, La_3InC, La_3InN.

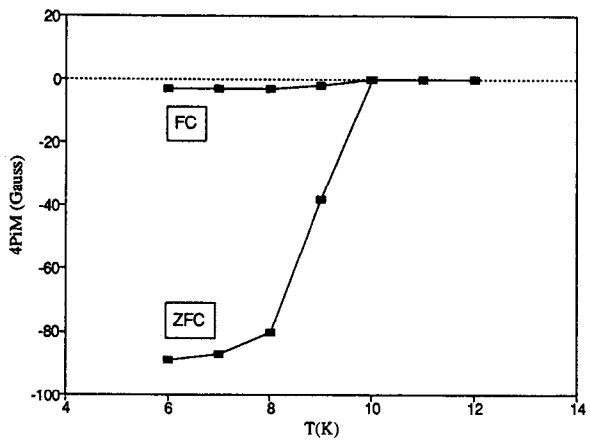

Fig. 3. Magnetization of La_3In at 6–12 K and 50 Oe when cooled in the magnetic field (FC) and in zero field (ZFC).

has been concluded to be intrinsic [7]. Low field (50 Oe) measurements show a superconducting transition at about 10 K, Fig. 3, both when field-cooled (FC) and when zero-field-cooled (ZFC). The supercurrent shielding, Table 5, is characteristic of superconductors [7].

La_3InB: Surprisingly, the unit cell parameters and T_c values of the boride samples neither differ significantly from those of binary La_3In nor change appreciably with boron content (Tables 1 and 5). The room temperature susceptibilities are somewhat greater than those of La_3In, Fig. 4(a). (The increases in χ at 3 T in several systems below about 50 K probably arise from paramagnetic (or other) impurities.) The measured supercurrent shielding increases somewhat with the boron content (Table 5 and Fig. 4(b)). The second La_3InB, and La_3InC, samples listed illustrate how unsatisfactory their syntheses are without the powder sintering step, especially in the magnetic data. No extra lines were observed in the powder patterns following the two boride powder sintering reactions with $x \leq 1$. The foregoing, fairly unchanging, physical properties naturally lead to some concern and uncer-

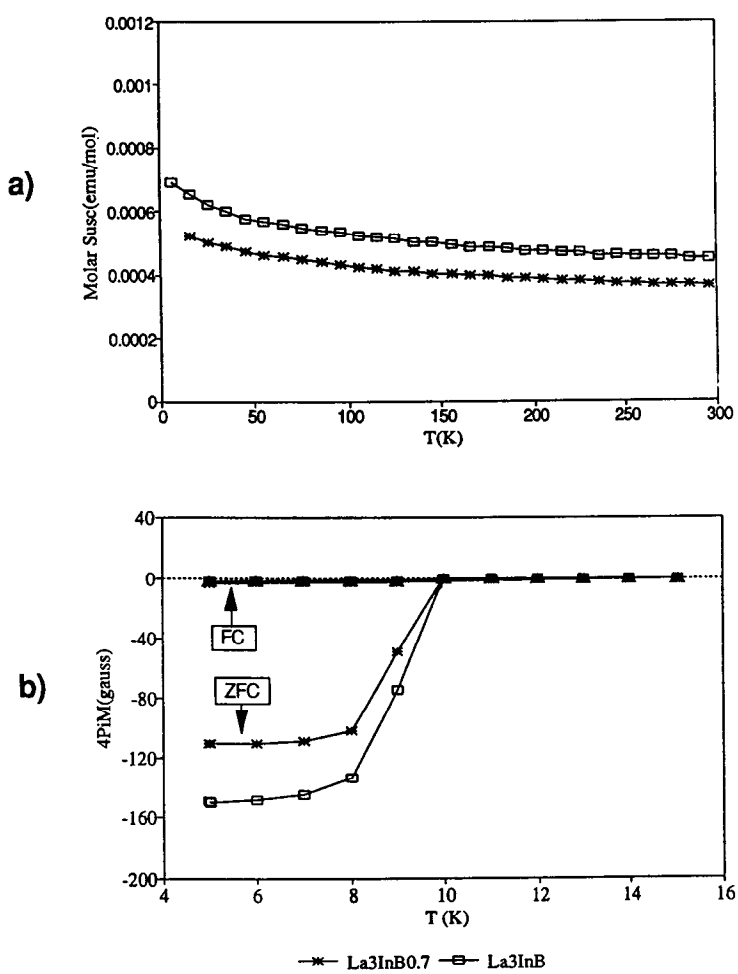

Fig. 4. (a) Magnetic susceptibilities (b) and magnetization data for $La_3InB_{0.7}$ and La_3InB.

tainty about the actual incorporation of the boron interstitial. An SEM-EDX examination of the first La_3InB sample listed also confirmed a single phase product with the proper boron content. This is also consistent with our general experiences in other systems, La_5Ge_3Z for example [10], according to which the reaction of free boron (or other Z) with the lanthanum-rich La_3In at 1200°C would, in the absence of compound formation, be expected to yield LaB_x and La_2In (or a lanthanum-poorer ternary phase). Note that La_2In did appear with a $La_3InB_{1.5}$ composition (Table 1). The evidence is that boron is truly bound in the La_3In structure up to about the La_3InB stoichiometry.

La_3InC: As with yttrium, the unit cell parameters of the perovskite-like phase increase with increasing carbon content. The largest change occurs within the first 0.3 increment of carbon in La_3InC_x, which may span a two-phase region (at room temperature). The system appears to be single phase from $La_3InC_{0.3}$ to La_3InC, although the appearance of a small amount of another phase at the monocarbide composition may indicate that the upper limit is slightly lower. The La–C distances (equal to $a/2$) in different samples are in the neighborhood of 2.59 Å; the same as can be deduced from a number of $Zr_6(C)Cl_{12}$ cluster halide analogues [21] after the average of a narrow range of Zr–C distances, 2.28 Å, is corrected by the difference in six-coordinate crystal radii for Zr^{IV} vs. La^{III} [22]. The brittleness of the samples suggest that the bonding is dominated by La–C.

The perturbations provided by carbon lead to distinct modifications of the superconducting and susceptibility properties, Fig. 5 and Table 5, increasing amounts of carbon decreasing T_c, the supercurrent shielding, and normal-state χ, which are all Pauli in character. The superconductivity disappears in the La_3InC composition prepared by the same powder sintering method, while a small remnant in a second sample prepared by direct fusion and annealing suggests some carbon loss may have occurred. Heiniger, et al. [7] have reported the absence of superconductivity (greater than 1.02 K) for a La_3InC sample with a lattice constant of 5.19 Å, in reasonable agreement with ours. They also determined a distinct drop in the electronic specific heat relative to La_3In (14.0 → 5.9 mJ mol^{-1} K^{-2}). The apparently diminished density of

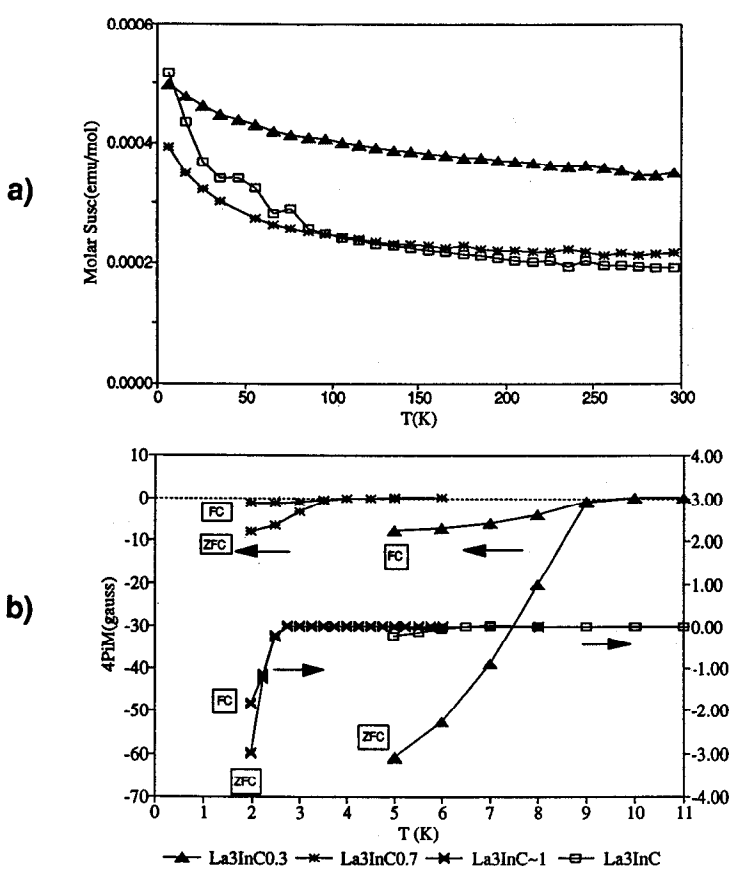

Fig. 5. (a) Magnetic susceptibilities (b) and magnetization data for La_3In_x as a function of temperature and x. The data for $La3InC_{\sim 1}$ in the latter refer to the second monocarbide sample in Tables 1 and 5. Note the expanded ordinate scale of the monocarbides.

states at E_F (judging from χ_{RT}) again suggests the monocarbide is approaching a valence compound, as reflected in the (extreme) assignment of oxidation states as $(La^{+3})_3In^{-5}C^{-4}$. The resistivity measurements for La_3InC by the Q-method indicate it is a somewhat poor metal, with a room temperature value near 52 $\mu\Omega \cdot$ cm and a temperature coefficient of 0.08% K^{-1}.

La_3InN: The antiperovskite structure of La_3InN was refined from single crystal data to confirm that stoichiometric amounts of nitrogen occupy the centers of the La octahedra and that the indium atoms occupy the centers of the La cuboctahedra. The La–N interatomic distance found, 2.5510 Å, is notably less than either that in LaN (NaCl type) [23] or the sum of atomic radii [16], both of which are 2.65 Å, but it is quite reasonable relative to the observed La_3InC value (2.60 Å). Some constriction of the f.c.c. La lattice and thence of LaN is to be expected on substitution of the smaller indium atoms on one-fourth of the lanthanum sites. The superconducting property is absent (above 2 K) for the mononitride (other compositions were not investigated), while the normal-state magnetic susceptibility is small and Pauli in character, Fig. 2, with a negligible temperature dependence. An analogous compound did not form with phosphorus.

La_3InO: Cell dimensions of the oxide samples indicate that the electron-richest Z example is effectively the same size as carbon, but that there is very little dependence of cell size on composition beyond $La_3InO_{0.3}$. Slightly reduced yields at the monoxide composition suggest that the stoichiometry range may not extend to full occupancy. The La–O distances are near 2.60 Å, relative to a 2.54 Å average with seven neighbors in La_2O_3 [24]. Strikingly, the introduction of the oxygen into the structure does not change the superconducting temperature very much, but it decreases the supercurrent shielding fairly regularly, Table 5 and Fig. 6. The normal-state magnetic susceptibilities remain high and Pauli in character, with

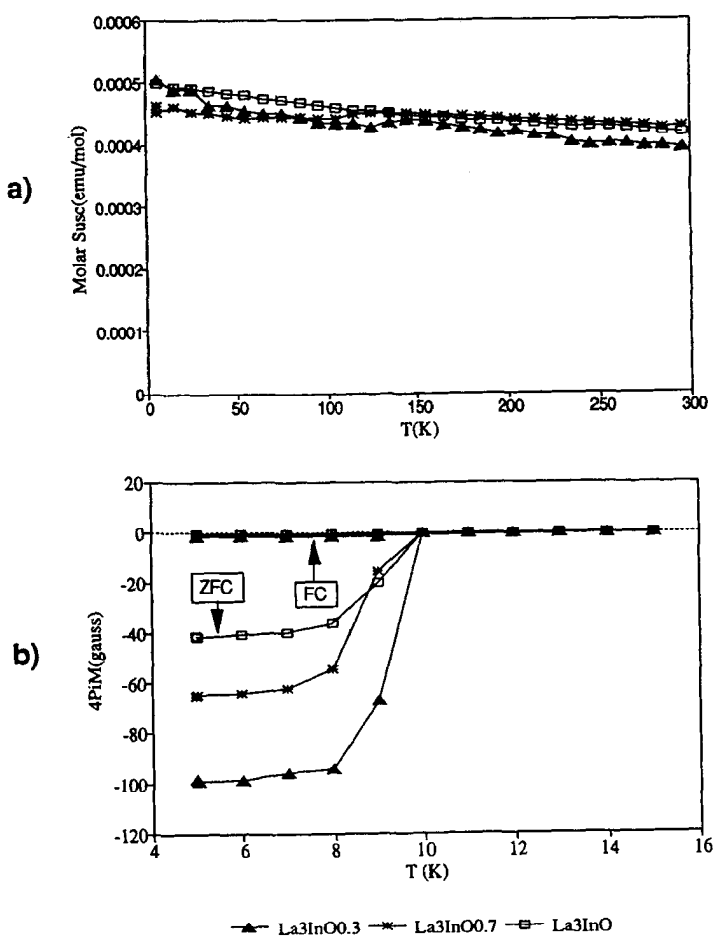

Fig. 6. (a) Magnetic susceptibilities (b) and magnetization data for La_3InO_x, $0.3 \leq x \leq 1.0$.

about the smallest temperature dependence seen except for La_3InN.

The change of f.c.c. La ($a = 5.29$ Å) into La_3In through replacement of one-fourth of the atoms (the cell corners) by the smaller In is generally accepted to be the source of the accompanying cell contraction ($a = 5.09$ Å) [7]. In fact, $La_3T\ell$ behaves very similarly ($a = 5.06$ Å) [25]. (The contrasting $a = 5.66$ Å reported for La_3Ga [26] seems improbable, and we have been unable to reproduce the synthesis, obtaining only La_5Ga_3 and La on slow cooling. A T_c of 5.8 K was reported sometime ago for a sample of this composition with an unspecified phase composition or structure [27]. Impurity interstitials may again be involved.) The subsequent insertion of the interstitial Z into the lanthanum octahedron in (the body center of) La_3In adds a strong heteropolar bonding component and, presumably, a stiffening of the lattice. The same B, C, N, O interstitials are well recognized for their strong bonding within, even contracting effects on, the confacial trigonal antiprisms of transition metals that are present in the common Mn_5Si_3-type structures of, among others, La_5Tt_3, Tt = Ge, Sn, Pb [10,11] and Zr_5M_3, M = Sb, Si, Sn, Pb [8,28–30]. The contrasting lack of regular trends in properties that we have observed among the La_3InZ compounds are a most striking feature of the present investigation. We have therefore paid particularly careful attention to ensure that the reported effects are real, without encountering any evidence that they are not.

Table 6 summarizes the various physical properties of La_3In and the fully stoichiometric La_3InZ phases (made under uniform synthetic conditions). The generalities are as follows. In the end members, B and O have only small effects on T_c; nonetheless, these Z respectively increase and decrease the supercurrent shielding by somewhat over 50%, and this varies inversely with the volume changes, namely, near zero

Table 6
Property variations among $La_3InZ_{1.0}$ phases

Z	La_3In	La_3InB	La_3InC	La_3InN	La_3InO
V_{cell} (Å^3)	131.8	132.3	140.4	133.4	140
$-\Delta V$ (Å^3)	—	0.5	8.6	1.6	8
T_c (K)	10	10	<2	<2	10
Supercurrent shielding (%)	180	300	—	—	80
$10^4\ \chi_M$ (293)	3.8	4.6	2.0	1.5	4.3
μ_{eff} (BM)	1.9	1.8	1.2	—	2.8

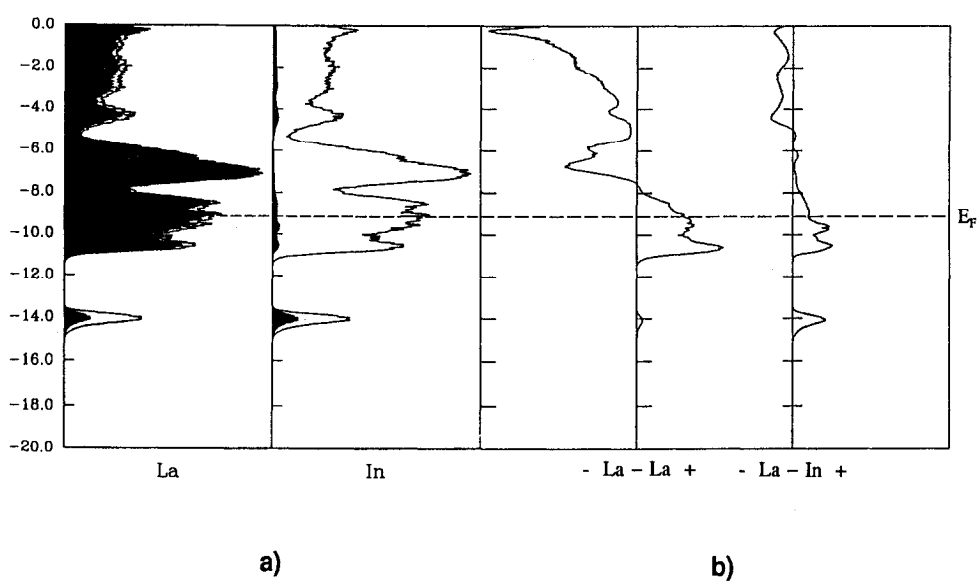

Fig. 7. Extended Hückel band calculational results for La_3In (E_F dashed). (a) Total DOS with La and In contributions projected out; (b) COOP data for pairwise La–La and La–In overlap-weighted populations. + denotes bonding and − antibonding.

(B) and +6% (O). In contrast, both C and N quench the superconductivity (above 2 K) while giving divergent (about 6.5% and about 1.2%) volume increases, although the latter more or less follows normal radius expectations. The best correlation turns out to be an inverse relationship between T_c and χ_{RT}, i.e. $T_c < 2$ K when $10^4\chi_{RT} \leq 2.0$ while all $T_c \geq 9$ K had $\chi_{293} > 3 \times 10^4$ emu mol^{-1} except for the La_3InB sample prepared by a poorer method. The higher susceptibilities of course presumably reflect something of larger room temperature densities-of-states at E_F. The susceptibility of normal Y_3InC is somewhat less than that of La_3InC, but there is no binary host with which to compare the former. All of the nonsuperconducting products are distinctly more brittle, while the superconducting La_3In, La_3InB and La_3InO are more metal-like physically.

Band calculations: Some of the rather unusual trends revealed by the above data are a little more reasonable, or plausible, when the results of extended Hückel band calculations for all five materials are considered. Of course, these are not sufficient to explain superconductivity or not, but some differences are evident. All calculations pertain to the observed lattice dimensions.

In all cases, E_F falls in a broad band with major La–La bonding contributions. The contributions by In in this region, and the results of the addition of increasingly electronegative Z are illuminating. There is a noticeable In component at E_F in La_3In, Fig. 7, and this narrows appreciably when B is bound; however, a maximum in La–In bonding remains close by. The antibonding t_{1u} states about the interstitial vacancy in La_3In (at Γ) lie in the large band near −7 eV. When the cavity is filled by B, La d–B p interactions split this into bands at −9.5 eV and −6.5 eV (at Γ), while the intervening states are nearly all La d and s. Significant dispersion broadens all of these. Many of the differences seen with subsequent Z result from the tighter bonding of the t_{1u} level. In La_3InB, broad B and La–B bonding contributions occur at and just below E_F, Fig. 8. The horizontal dashed lines shown represent E_F levels for La_3InB_x at $x = \frac{1}{4}, \frac{1}{2}, \frac{3}{4}, 1$ on the assumption of a rigid band. The apparent decrease in DOS with the increasing x is not particularly reflected in the T_c data, Table 6, but this is a particularly high DOS.

The p-orbital-based levels of Z for subsequent elements fall rapidly so that even carbon 2p is important only in the valence region, well below E_F. (E_F also rises as we add electron-richer Z.) As a result, there is a distinct fall in DOS at E_F between B and C, as also observed in χ_{RT}. (The abscissa scaling in Figs. 7–11 is arbitrary but the In 5s band sizes at −14.0 eV in Figs. 8 and 9 give a reasonable comparison.) Furthermore, the rough composition dependence of DOS at E_F on carbon content correlates well with the distinct parallel decrease observed in T_c. The maximum In contribution and La–In bonding near E_F also fall in energy, an effect that is particularly noticeable by nitrogen. Here, the In 5s and N 2p levels also fall near one another, and there is significant mixing of La at this energy (Fig. 10). The occurrence of separate N 2s (not shown), In 5s, N 2p bands as well as In 5p just below E_F are, even with a broad overarching La conduction band, in the spirit of a 'metallic Zintl phase' [20] character for La_3InN. Finally, in the larger

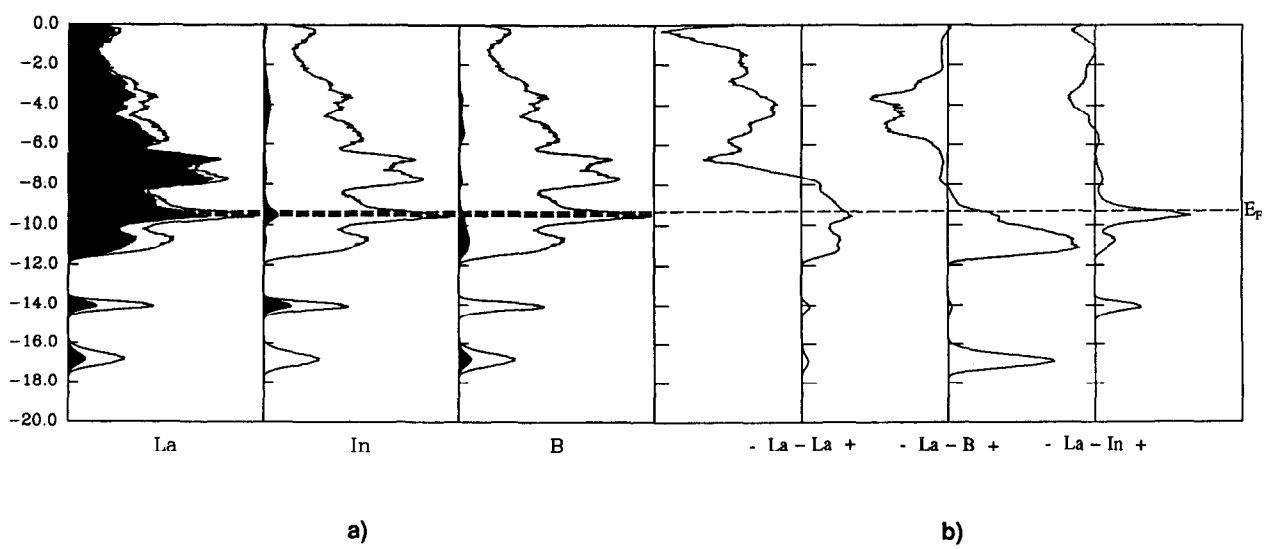

Fig. 8. Band calculational results for La_3InB. (a) Total DOS with individual atoms contributions projected out. The dotted lines mark the rigid bond approximations for 1/3, 2/3 and full B occupancies (13,14,15 e$^-$); (b) COOP curves for specified pairwise interactions.

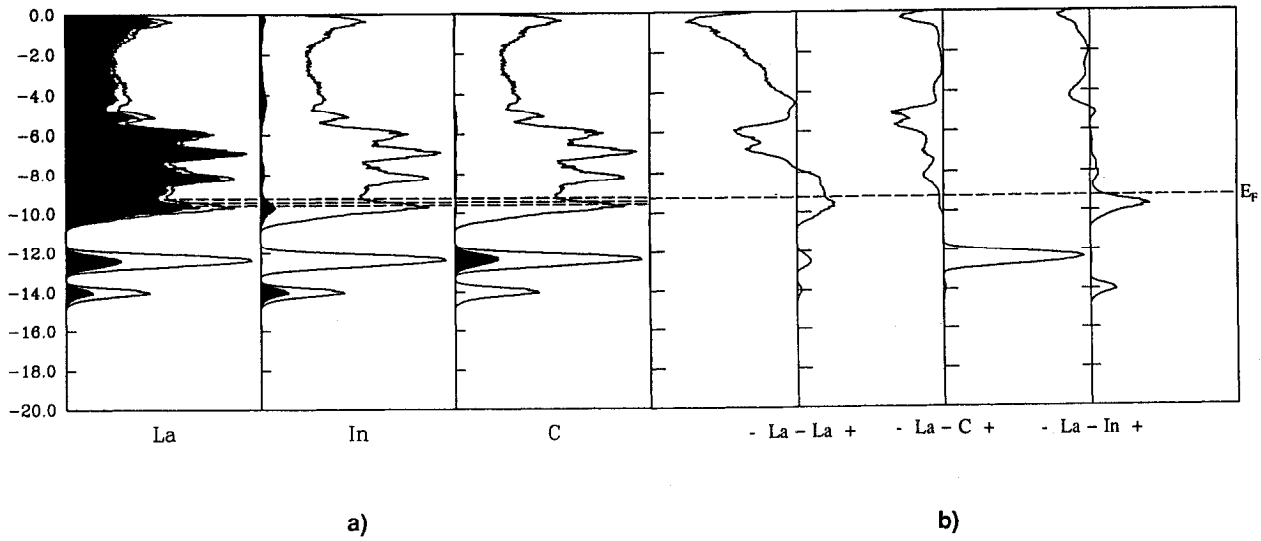

Fig. 9. Band calculational results for La_3InC. (a) Total DOS with individual atoms projected out and E_F estimated for 1/2, 3/4 and full C occupancies (14,15,16 e^-); (b) COOP curves for the indicated interactions.

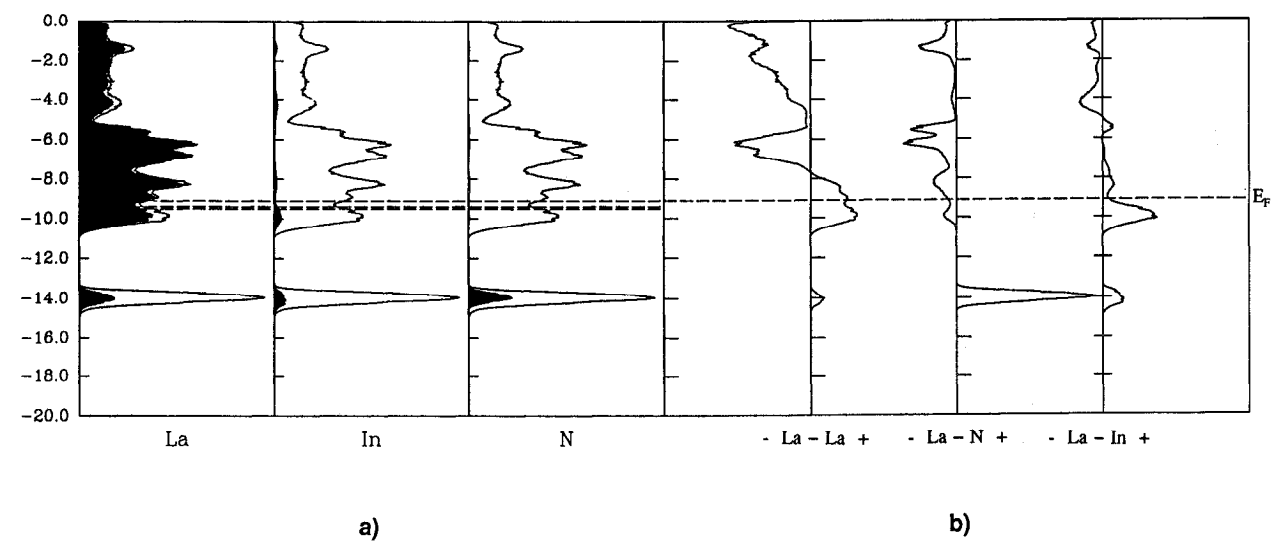

Fig. 10. Band calculational results for La_3InN. (a) Total DOS with individual atoms projected out and E_F estimated for 3/5, 4/5 and full C occupancies (15–17 e^-); (b) COOP curves for the indicated interactions.

oxide, somewhat more antibonding La–O interactions appear around E_F, and the La–In interactions increase and broaden around E_F, reminiscent of, but smaller than, the effects seen at the beginning of the series. Another electron is added to the conduction band too. It is of course still difficult to say that these changes are responsible for the observed T_c enhancement. The dependence of DOS at E_F on oxygen concentration seems small. It is worth noting that the two phases that show no superconductivity, La_3InC and La_3InN, have more traditional valence properties and are also brittle, while the ternary superconductors remain physically more tough and metal-like.

Acknowledgement

D.K. Finnemore provided valuable guidance as well as support of the magnetic measurements, and the authors are also indebted to H.F. Franzen for the use of arc-melting and induction furnaces. This research was supported by the Office of the Basic Energy

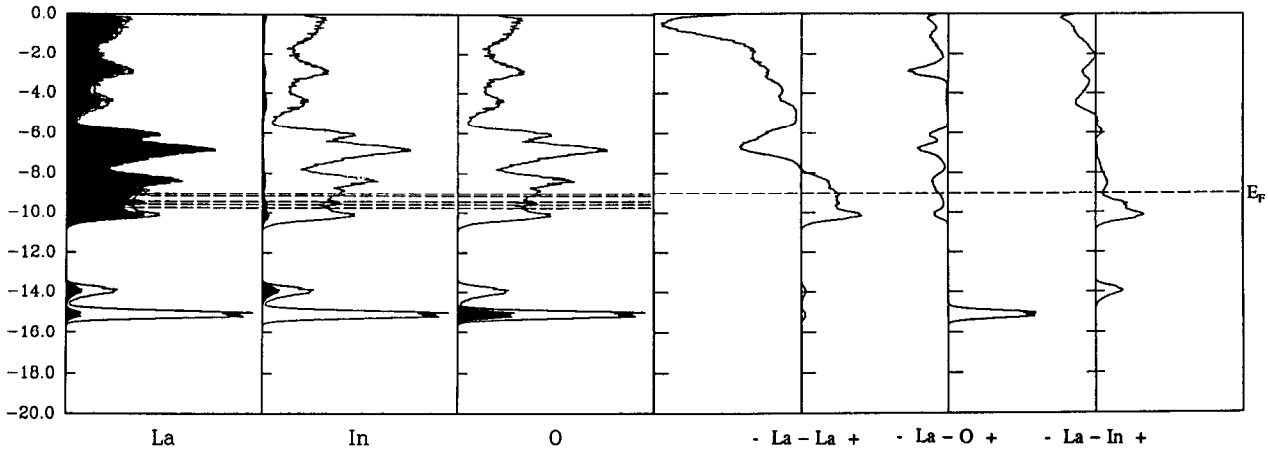

Fig. 11. Band calculational results for La_3InO. (a) Total DOS with individual atoms projected out and E_F estimated for 1/3, 1/2, 2/3, 5/6 and full O occupancies; (b) COOP curves for the indicated interactions.

Sciences, Materials Sciences Division, Department of Energy. The Ames Laboratory is operated for DOE by Iowa State University under Contract No. W-7405-Eng-82.

References

[1] H. Nowotny, *Proc. Seventh Rare Earth Research Conf., Coronado, California, 1969*, p. 309.
[2] S.P. Yatsenko, A.A. Semyannikov, H.O. Shakarov and E.G. Fedorova, *J. Less-Common Met., 90* (1983) 95.
[3] W. Jeitschko, H. Nowotny and F. Benesovsky, *Monatsh. Chem., 95* (1964) 1040.
[4] H. Haschke, H. Nowotny and F. Benesovsky, *Monatsh. Chem., 97* (1966) 716.
[5] H. Haschke, H. Nowotny and F. Benesovsky, *Monatsh. Chem., 98* (1967) 2157.
[6] B.T. Matthias, V.B. Compton and E. Corenzwit, *Phys. Chem. Solids, 19* (1961) 130.
[7] F. Heiniger, E. Bucher, J.P. Maita and P. Descouts, *Phys. Rev. B, 8* (1973) 3194.
[8] E. Garcia and J.D. Corbett, *Inorg. Chem., 29* (1990) 3274.
[9] O.D. McMasters and K.A. Gschneidner, Jr., *J. Less-Common Met., 38* (1974) 137.
[10] A.M. Guloy and J.D. Corbett, *Inorg. Chem., 32* (1993) 3532.
[11] A.M. Guloy and J.D. Corbett, *J. Solid State Chem., 109* (1994) 352.
[12] J.T. Zhao and J.D. Corbett, *J. Alloys Comp., 210* (1994) 1.
[13] TEXSAN, Version 6.0, 1990, Molecular Structure Corporation, The Woodlands, TX.
[14] N. Walker and D. Stuart, *Acta Crystallogr. Sect. A:, 39* (1983) 158.
15 J. Shinar, B. Dehner, B.J. Beaudry and D.T. Peterson, *Phys. Rev. B, 37* (1988) 2066.
[16] T. Hughbanks and R. Hoffmann, *J. Am. Chem. Soc., 105* (1983) 3531.
[17] J.C. Slater, *J. Chem. Phys., 41* (1964) 3199.
[18] S.M. Kauzlarich, M.W. Payne and J.D. Corbett, *Inorg. Chem., 29* (1990) 3777.
[19] S.M. Kauzlarich, T. Hughbanks, J.D. Corbett, P. Klavins and R.N. Shelton, *Inorg. Chem., 17* (1988) 1791.
[20] J.-T. Zhao and J.D. Corbett, *Inorg. Chem., 34* (1995) 378.
[21] R.P. Ziebarth and J.D. Corbett, *J. Am. Chem. Soc., 111* (1989) 3272.
[22] R.P. Shannon, *Acta Crystallogr. Sect. A:, 32* (1976) 751.
[23] U. von Essen and W. Klemm, *Z. Anorg. Allg. Chem., 317* (1962) 25.
[24] P. Aldebert and J.P. Traverse, *Mater. Res. Bull., 14* (1979) 303.
[25] L.S. Nalatnik and I.I. Fal'ko, *Dokl. Akad. Nauk SSSR, 241* (1978) 828.
[26] S.P. Yatsenko, A.A. Semyannikov, B.G. Semenov and K.A. Chuntonov, *J. Less-Common Met., 64* (1979) 185.
[27] T.F. Smith and H.L. Luo, *J. Phys. Chem. Solids, 28* (1967) 569.
[28] Y.-U. Kwon, M.A. Rzeznik, A. Guloy and J.D. Corbett, *Chem. Mater., 2* (1990) 546.
[29] Y.-U. Kwon and J.D. Corbett, *Chem. Mater., 4* (1992) 1349.
[30] Y.-U. Kwon and J.D. Corbett, *J. Alloys Comp., 190* (1993) 219.